Applied Catalysis B: Environmental 217 (2017) 523–529

Contents lists available at ScienceDirect

Applied Catalysis B: Environmental

journal homepage: www.elsevier.com/locate/apcatb

Control the energy band potential of ZnMgO solid solution with enhanced photocatalytic hydrogen evolution capacity

Hongwei Wang [a], Wenqiang Zheng [b], Weibing Li [b], FengHui Tian [a,**], Shaoping Kuang [b,***], Yuyu Bu [a,c,*], Jin-Ping Ao [c]

[a] College of Environment & The Cultivation Base for State Key Laboratory, Qingdao University, No. 308 Ningxia Road, Qingdao, 266071, PR China
[b] College of Environment and Safety Engineering, Qingdao University of Science and Technology, No. 53 Zhengzhou Road, Qingdao, 266042, PR China
[c] Institute of Technology and Science, Tokushima University, 2-1 Minami-Josanjima, Tokushima 770-8506, Japan

ARTICLE INFO

Article history:
Received 11 January 2017
Received in revised form 5 April 2017
Accepted 9 April 2017
Available online 4 June 2017

Keywords:
Energy band control
ZnMgO
Solid solution
Photocatalysis
Hydrogen evolution

ABSTRACT

In this study, we prepared a novel hierarchic nanorod ZnMgO solid solution photocatalyst, and in the crystal, part of Zn atoms were replaced by Mg atoms. Experimental results and theoretical calculation data firstly indicated that the energy band structure of the ZnO can be tuned with the Mg elements doping in it. Especially, during this process, the conduction band (CB) potential of ZnMgO solid solution moved to more negative site gradually with the Mg content increasing, which is an important characteristic for n-type water splitting photocatalyst. When the mole ratio of Mg in the reaction solution reach to 50%, corresponding end-product ZnMgO showed a much more negative CB potential (−0.46 V vs NHE) than pure ZnO (−0.05 V vs NHE), and the photocatalytic for hydrogen evolution product of ZnMgO solid solution increased dramatically than pure ZnO (from near zero of ZnO to 1103.9 μmol/g in 4 h). Furthermore, in the future, based on the ZnMgO solid solution prepared in this study, more visible-light-responsive solid solution with suitable water splitting band structure, such as ZnMgON and ZnMgOS etc., can be expected.

1. Introduction

ZnO, a wide band gap (3.34 eV) semiconductor has been widely researched in photocatalytic areas, such as photocatalytic hydrogen evolution [1,2], organic pollutions degradation [3,4], antibacterium [5,6] and so on. Compared with TiO_2, the charge carriers mobility of ZnO is about two orders of magnitude larger than that of TiO_2. [7] Thus, ZnO may possess higher photoelectric conversion capability than TiO_2. However, to date, pure ZnO powder photocatalyst has not provided an excellent efficiency for photocatalytic hydrogen evolution from water. The most challenge is that the conduction band (CB) potential of ZnO is near the water reduction potential, so the overpotential of the photogenerated electrons by ZnO is too small to reduce the H^+ to H_2 quickly [8,9]. For promoting the over-potential of ZnO in this reaction process, the band structure of ZnO should be modified, especially negative move of the conduction band potential of it.

Recent years, many solid solution photocatalysts, such as GaZnON [10,11], $LaTiO_2N$ [12,13] and Bi_4NbO_8Cl [14] had been reported possession excellent photo to chemistry energy conversion efficiency. Contrary to ZnO, the fundamental working mechanism of these solid solution systems are that they have negative moved the valence band (VB) potential, meanwhile keep constant of the CB potential, which is negative enough for hydrogen evolution. Thus, on the one hand, the photo absorption range of the solid solution can be enlarged, on the other hand, the reduction capacity of the photogenerated electrons can be held at a relative high level, that to improve the photocatalytic performance of it.

However, generally, for a n-type solid solution photocatalyst, their CB potentials are not negative enough to limit their photocatalytic water splitting performance improving further [12,15,16]. In this article, we employed hydrothermal method to treat the Zn and Mg elements to form a ZnMgO precursor, subsequently, annealing the precursor to achieve a novel hierarchic nanorod ZnMgO soild solution with Mg substituting on Zn site. To date, Although some works have been reported the Mg doped ZnO photocatalysts, in these studies, the content of Mg is relative low and they never

* Corresponding author at: College of Environment & The Cultivation Base for State Key Laboratory, Qingdao University, No. 308 Ningxia Road, Qingdao, 266071, PR China.
** Corresponding author.
*** Corresponding author.
E-mail addresses: tfh@qdu.edu.cn (F. Tian), kuangshaoping@126.com (S. Kuang), buyuyuqust@163.com (Y. Bu).

http://dx.doi.org/10.1016/j.apcatb.2017.04.079
0926-3373/

analysis the photocatalysis mechanism from the angle of energy band structure [17–19]. In this study, from the research results we found that with the Mg contents of the ZnMgO increasing, the corresponding CB negative move gradually, to enhance the reduction capacity of photogenerated electrons of the ZnMgO. So, this is a facile method to negative move the CB potential of ZnO, meanwhile, not enlarge the band gap width greatly of it. In addition, compared with GaZnON, $LaTiO_2N$ and Bi_4NbO_8Cl etc., there are no expensive elements bonding in ZnMgO. Furthermore, ZnMgO has a potential to dope N and S elements, that to form a ZnMgON and ZnMgOS visible light responsive photocatalyst. Thus, ZnMgO solid solution preparing in this study is a potential material for fabricating cheap, stable water splitting photocatalyst further, which possesses negative enough CB potential, meanwhile response in visible light area.

2. Experimental

2.1. Preparation of pure ZnO and ZnMgO hierachical nanorods

All the materials were purchased from Sinopharm Chemical Reagent Co., Ltd. (Shanghai, China) and used as received without further purification. For preparation of ZnO nanorods, As shown in Schematic S1, dissolution of 10 mmol $Zn(NO_3)_2{\cdot}6H_2O$ and 10 mmol $H_2C_2O_4$ into 20 mL ethanol, respectively. After dissolving completly, pour the $H_2C_2O_4$-ethanol solution into the $Zn(NO_3)_2$-ethanol solution quickly with a strong stirring to form a homogeneous colliod. Then, The colliod was transferred into a 100 mL Teflon-lined stainless-steel autoclave, and heated at 130 °C for 10 h. After that, the liquid mixture was centrifugalized and repeatedly washed with deionized water and anhydrous ethanol, then dried at 80 °C for 24 h. Finally, the dried powder was annealed at 420 °C for 2 h to get the white powder. For preparating ZnMgO with different Mg contents, amount of $Zn(NO_3)_2{\cdot}6H_2O$ were replaced by $Mg(NO_3)_2{\cdot}6H_2O$ (Mg^{2+} occupy 30%, 50% and 70% ratio to the total mole of the metal ions) to dissolve into the ethanol solution. And other procedures kept the same with the pure ZnO preparation process. The corresponding ZnMgO solid solutions marked as 30-ZnMgO, 50-ZnMgO and 70-ZnMgO. The real elements ratios of Mg and Zn in 30-ZnMgO, 50-ZnMgO and 70-ZnMgO samples were tested by atomic absorption spectrum, and the results are presented in Table S1.

2.1.1. Characterization

X-ray diffraction (XRD, D/MAX-2500/PC; Rigaku Co., Tokyo,Japan) was used to identify the crystalline structures of the series samples. The morphology of the prepared samples was analyzed using a scanning electron microscope (SEM, JSM-6700F; JEOL, Tokyo,Japan). The bond state of the synthesized materials were analyzed using X-ray photoelectron spectroscopy (XPS, Axis Ultra, Kratos AnalyticalLtd., England). The morphology of the series samples was observed using field emission transmission electron microscope (FE-HRTEM, Tecnai G2 F20, FEI Company, USA). UV–vis diffuse reflectance spectrophotometer (U-41000; HITACHI, Tokyo, Japan) was used to study the optical absorption properties of the series samples. The photolumines-cence intensity and excited state electron radioactive decay of theprepared photocatalysts were characterized using a fluorescencespectrometer (PL, Fluoro Max-4, HORIBA Jobin Yvon, France).

2.1.2. Assessment of the photocatalytic hydrogen evolution and apparent quantum efficiency (AQE) performances of these photocatalysts

In this test, 0.1 g photocatalyst was added into a mixture including 10 mL methanol and 90 mL deionized water. Then 1 wt% $HPtCl_4$ added into the mixture. A 150 W Xe lamp (PLS-SXE300, Beijing Changtuo Co. Ltd., China) was used as white light source, and the light density at the liquid surface was 250 mW/cm^2. The testing temperature was maintained at 5 °C by condensate water system.

The AQE performances of pure ZnO, 30-ZnMgO, 50-ZnMgO and 70-ZnMgO photocatalysts were tested under various wavelengths (300 nm, 365 nm, 385 nm, 405 nm and 430 nm, Zaher, Germany) light illumination. The incident light intensity was measured using a spectroradiometer (Thorlabs, PM100D). And the AQEs were calculated according to the following Equ.

$$AQE = 2 \times numberofevolvedH_2nolecules/numberofincidentedphotons$$

2.1.3. Electrochemical measurements

The photoelectrode was prepared by dip-coating method. Simply, 50 mg photocatalyst powder are ground,and dissolved with 5 mL alcohol to get a sol, then coat 20 μL prepared sol on a clean FTO with an active area 1 cm × 1 cm. Lastly, it was annealed under 350 °C in air for 1 h. Electrochemical measurements were performed in a traditional three-electrode experimental system by CHI660D Electrochemical Workstation (Shanghai Chenhua Instrument Co., Ltd., Shanghai, China). The prepared series photoelectrodes, Ag/AgCl, and Pt electrode acted as the working, reference, and counter electrodes, respectively. Electrochemical impedance spectroscopy (EIS) tests were performed at 0 V vs Ag/AgCl over the frequency range between 10^4 and 10^{-1} Hz, with an AC voltage magnitude of 5 mV, using 12 points/decade. Mott-Schottky plots was measured at the potential range of −1.6 V to −0.2 V and the frequency of 10 Hz with an AC voltage magnitude of 10 mV. All tests were carried out in 0.5 mol L^{-1} Na_2SO_4 electrolyte.

2.1.4. Calculation details

The structures of the Zn-Mg-O were optimized based on density functional calculations by using the CASTEP code with the core orbitals replaced by ultrasoft pseudopotentials, and a kinetic energy cutoff of 310 eV. Exchange and correlation effects were described by the Perdew–Burke–Ernzerhof (PBE) generalized gradient approximation (GGA). The bulk ZnO was relaxed using 300 eV energy cutoff, and a 7 × 7 × 4 Monkhorst-Pack k-point mesh was employed. Both the atoms and the cell were allowed to relax. The energy, force, stress and displacement convergence criteria were set to 2.0×10^{-5} eV, 5.0×10^{-2} eV/Å, 0.1 GPa, and 2.0×10^{-3} Å, respectively. The structural model of Mg-doped ZnO was built by substituting Zn atom in a (2 × 2 × 2) supercell of ZnO with Mg atom (Fig. 4). The doping level of about 31.25%, 50.00% and 61.85% are considered and denoted as 30-ZnMgO, 50-ZnMgO and 70-ZnMgO, respectively. And k-point meshes of 4 × 4 × 2, 4 × 3 × 2 and 3 × 3 × 2 were used for 30-ZnMgO, 50-ZnMgO and 70-ZnMgO, respectively.

3. Results and discussion

The XRD results of pure ZnO, 30-ZnMgO, 50-ZnMgO and 70-ZnMgO are show in Fig. 1. The pure XRD peaks of ZnO shows a typical wurtzite phase. However, with the added content of Mg in the ZnMgO solid solution increasing gradually, the XRD peak intensities of these samples decreased, indicating that the particle size of these samples decreased with the Mg added content increasing. It is worth noting that just the (002) face of the crystals moved to higher angle with the Mg added content increasing. This phenomenon means that the (002) face of the ZnO was influenced with the Mg element in the solid solution.

The SEM images of pure ZnO and 50-ZnMgO are shown in Fig. S1. We can find that both ZnO and 50-ZnMgO showed a rod-like structure, which was assembled by nano particles. In order to observe the hierarchical structure of these samples, the TEM technique was employed to test them, and the corresponding results are shown

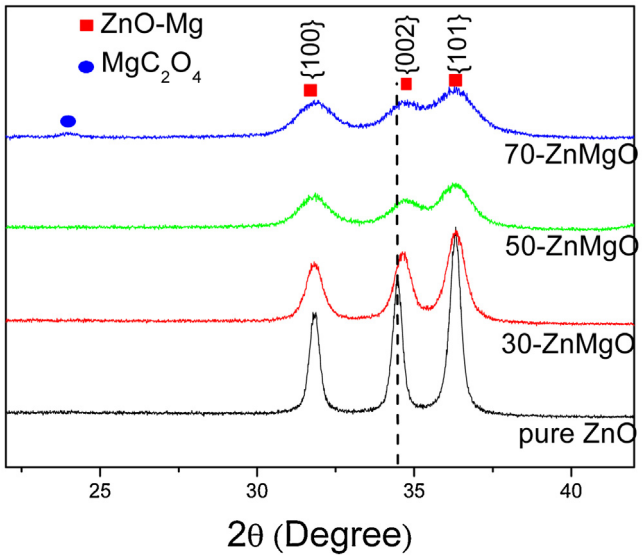

Fig. 1. XRD results of pure ZnO, 30-ZnMgO, 50-ZnMgO and 70-ZnMgO.

in Fig. 2. The TEM image of pure ZnO is shown in Fig. 2A, it can be found that the ZnO rod was formed by ZnO nanoparticles with a diameter approximately 20 nm. Fig. 2B shows the TEM image of 50-ZnMgO. Compared with pure ZnO, the nanoparticle size of 50-ZnMgO decreased to 5 nm, which is corresponding to the XRD results. This interesting phenomenon indicated that the crystal particle size of ZnMgO can be limited by doping in Mg element.

In order to research the band gap change of the ZnO and ZnMgO, the UV–vis DRS and Mott-Shottcky plots methods were employed to test these materials, and the results are shown in Fig. 3A and B. From Fig. 3A, it can be found that the band gap of pure ZnO prepared in this study was 3.18 eV (absorption threshold value is near 390 nm), however, with Mg added content increasing, the absorption threshold values were blue moved gradually, for the sample of 70-ZnMgO, the band gap width enlarge to 3.35 eV (absorption threshold value is near 370 nm). Fig. 3B presented the Mott-Schottcky plots of these samples. All the samples presented n-type semiconductor character, however, with Mg elements added content increasing in ZnMgO solid solution, the conducting band (CB) potential of the corresponding material is negative moved. This result demonstrated that the reduction capacity of the ZnMgO photogenerated electron is enhanced with the Mg content increasing. Combination the data providing in Fig. 3A and B, we summarized the energy band structure change situation, and the schematic is shown in Fig. 3C (all potential values translate from vs. Ag/AgCl into Normal Hydrogen Electrode (NHE)). From this result, we can find that the CB potential of pure ZnO is −0.05 V, of which value is very near the H^+ reduction potential, such a small overpotential limited the photocatalysis hydrogen evolution process. However, for the sample of 30-ZnMgO and 50-ZnMgO solid solutions, their CB potentials negative move to −0.44 V and −0.46 V respectively, these values are much higher than the H^+/H_2 hydrogen evolution potential, so this process of these two samples may be more smoother than that of pure ZnO. Further increase the Mg content, the CB potential of 70-ZnMgO negative move to −0.58 V. Thus, from the above results, we can conclude that Mg elements not merely enlarge the band gap width of ZnMgO solid solutions slightly, but negative move the CB potentials of them considerably, which may be an advantage for their photocatalytic water reduction process.

The photocatalytic water reduction for hydrogen evolution property of these materials are shown in Fig. 3D. Pure ZnO presented a trace amount of hydrogen after 4 h illumination, thep-erformance is limited by the positive CB potential of it. Since the Mg element in the precursor occupied 10 wt%, the corresponding sample 10-ZnMgO presented a litter increase of the photocataytic hydrogen evolution amount, compared with pure ZnO. However, since the Mg increased to 30 wt%, the photocataytic hydrogen evolution amount increase to 814.7 μmol/g for 4 h. Further enhanced Mg added content, the sample of 50-ZnMgO provide the best photocatalytic hydrogen evolution performance, which can produce 1103.9 μmol/g hydrogen for 4 h. However, with the Mg added content increased further, this performance of the sample of 70-ZnMgO decreased to pure ZnO closely. The stability of photocatalytic water reduction performance of 70-ZnMgO was assessed, and the result showed in Fig. S2. The water reduction for hydrogen evolution experiment was carried out for 4 cycles, and the photocatalytic water reduction for hydrogen evolution property was not decreased obviously after 4 cycles testing, indicating that 70-ZnMgO possess an excellent stability during photocatalysis process. This phenomenon may contributed to the enhanced stability of ZnO hexagonal phase after Mg element alloyed in.

Thetwo questions should be noticed in Fig. 3D. The former one is that 70-ZnMgO possesses more negative CB potential than 30-ZnMgO and 50-ZnMgO, but why did its photocatalytic performance for hydrogen evolution decrease so dramatically. The another one is that the samples of 30-ZnMgO and 50-ZnMgO possesses very near CB potentials, but why the photocatalytic performances for hydrogen evolution different. In order to clarify the above questions, firstly, the electrochemical impedance spectroscopy (EIS) technique was employed to test the electron transfer capacity of these materials, as shown in Fig. S3A, with the Mg solifying into ZnO, the impedance arc of these ZnMgO samples are much higher than that of pure ZnO, indicating that the electron transfer capac-

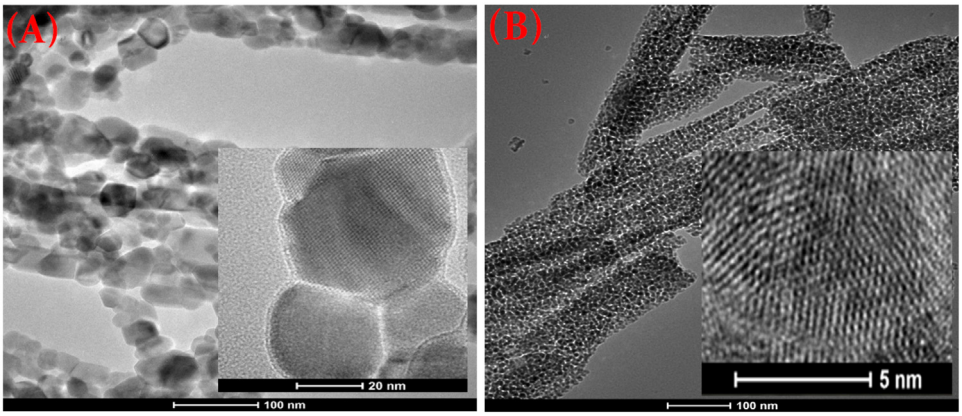

Fig. 2. TEM images of (A) pure ZnO and (B) 50-ZnMgO. Inserts is the corresponding high resolution image of both samples.

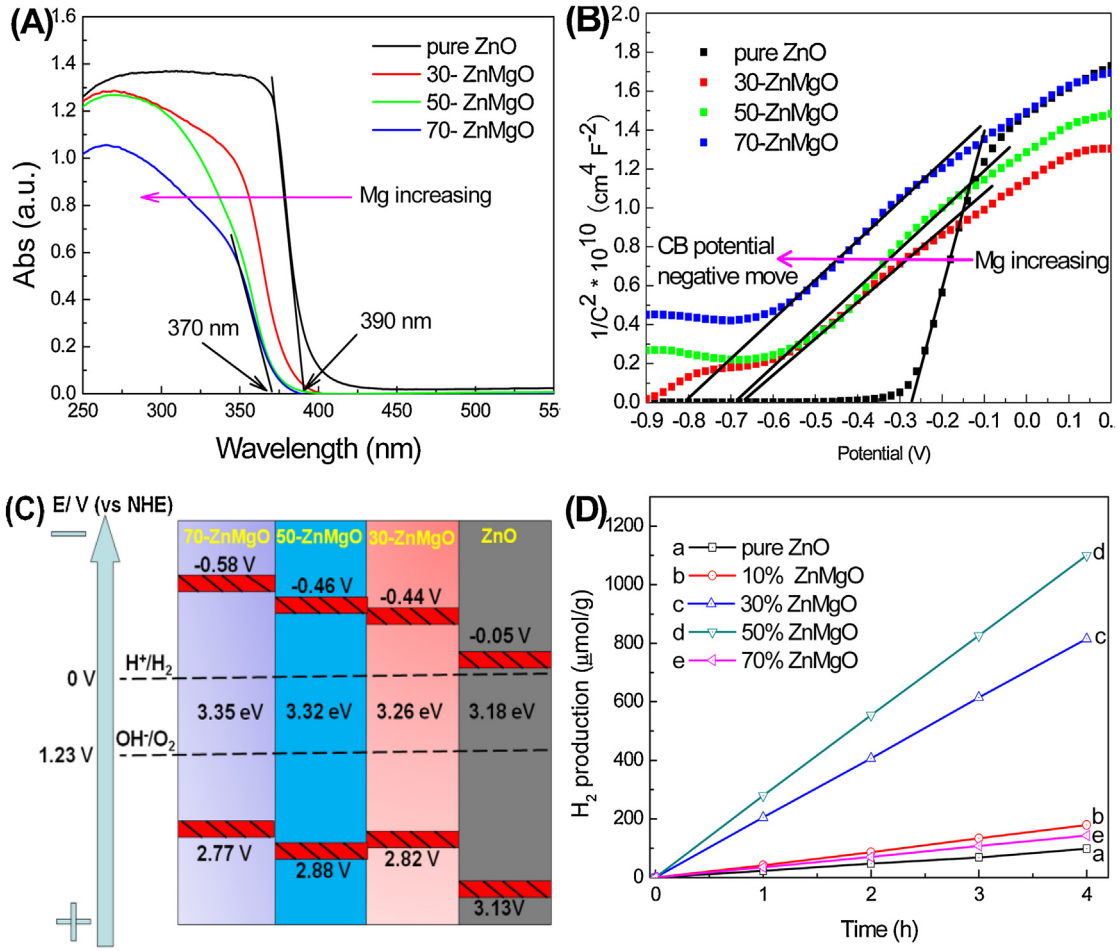

Fig. 3. (A) UV–vis diffuse reflection spectrum (DRS) and (B) Mott-Schottcky plots (vs Ag/AgCl) of ZnO, 30-ZnMgO, 50-ZnMgO and 70-ZnMgO; (C) Energy band structure schematic of these materials, which calculated from the data in (A) and (B); (D) photocatalytic water reduction for hydrogen evolution in 10 v% methanol solution, illuminated by a 150 W Xe light (250 mW/cm^2).

ity of ZnMgO solid solutions have not improved after Mg solid in. Fig. S3B presents the photoluminescence spectra (PL) of pure ZnO and series ZnMgO solid solutions. From PL results we can find that the pure ZnO, 30-ZnMgO and 50-ZnMgO presented same intensity of PL peaks at 704 nm, whereas, this peak intensity of 70-ZnMgO increased dramatically. The XPS C1s of 30-ZnMgO and 50-ZnMgO and 70-ZnMgO are shown in Fig. S3C.Comparing these results, we can find that the characteristic XPS background carbon peak present on 30-ZnMgO and 50-ZnMgO clearly. However, for the sample of 70-ZnMgO, this peak move to low energy direction, which corresponding to the Metal-C bond. Thus, combining with the XRD result, it can be confirmed that the MgC_2O_4 existed in 70-ZnMgO sample who induced the quick combination of photogenerated carriers, that to decrease the photocatalytic hydrogen evolution property dramatically of this sample. The surface oxygen bonds state of 30-ZnMgO, 50-ZnMgO and 70-ZnMgO had been tested, and the results are shown in Fig. S4. Comparing Fig. S4A and S4B, it is worth noting that the surface —OH ratio of 50-ZnMgO was enhanced significantly than that of 30-ZnMgO. As we known, surface —OH plays an important role on linking the water and the semiconductor surface, that to accelerate the hydrogen evolution process. Thus, for this reason, the 50-ZnMgO can provide a higher photocatalytic hydrogen evolution property than that of 30-ZnMgO. Fig. S4C is the O1 s curve of 70-ZnMgO, only C—O bonds can be found on this curve, indicating that MgC_2O_4 is coated on the surface of 70-ZnMgO.

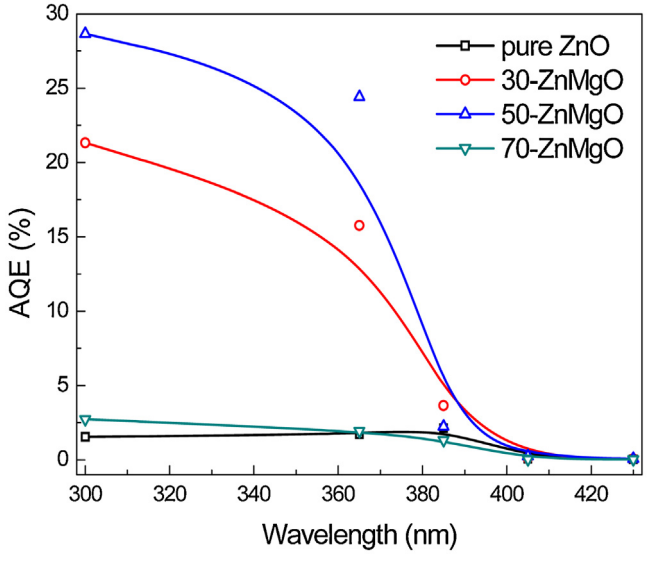

Fig. 4. Wavelength-dependent (300 nm, 365 nm, 385 nm, 405 nm and 430 nm) apparent quantum efficiency (AQE) of hydrogen evolution.

Additionally, the wavelength-dependent AQE of hydrogen produced by these photocatalysts is presented in Fig. 4. From this result, the samples of 30-ZnMgO and 50-ZnMgO presented much

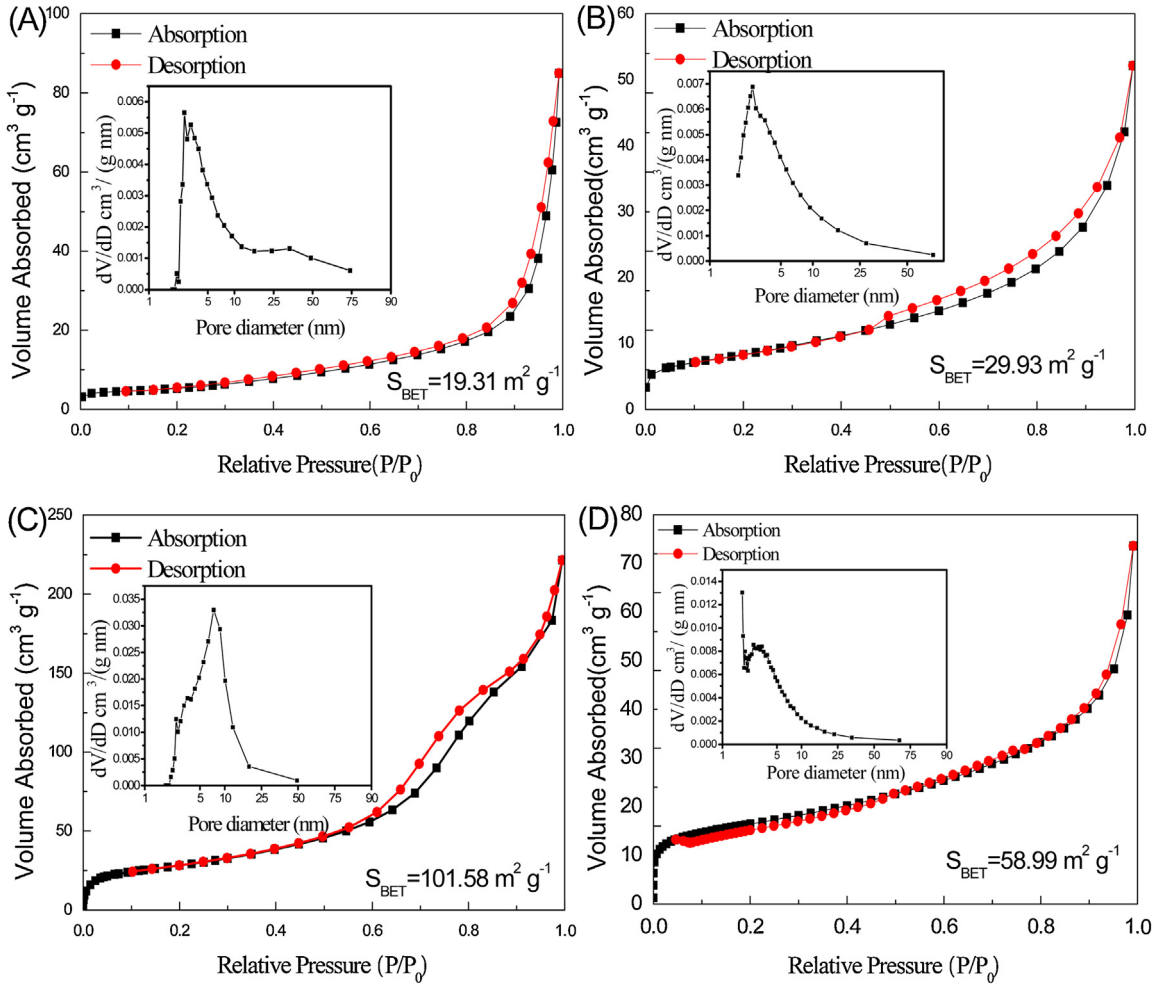

Fig. 5. N_2 adsorption/desorption isotherms of the (A) pure ZnO; (B) 30-ZnMgO; (C) 50-ZnMgO; (D) 70-ZnMgO. Insets are the corresponding pore size distribution.

higher AQE values than that of pure ZnO and 70-ZnMgO, the result accord with the photocatalytic hydrogen evolution performance shown in Fig. 3D. the sample of 50-ZnMgO perform on highest AQE performance. The AQE values located at 28.6% and 24.4% by 300 nm and 365 nm UV light illuminate, respectively. However, with the light wavelength red moving to 385 nm, corresponding AQE value decreased dramatically. In this case, the 50-ZnMgO presented a great photocatalytic hydrogen evolution performance, however, the AQE value is still low. So, there is large space to improve the photocatalytic hydrogen evolution performance of this material further.

From the HRTEM shown in Fig. 2, we can find that the particle size of 50-ZnMgO was decreased to quantum size with the Mg element doping in. The surface area of these samples would be changed with the content of Mg changing. So, we tested the BETs of these samples, and the results are shown in Fig. 5. From Fig. 5A–D, we can find that among the surface area value of these four samples, the values' order is 50-ZnMgO ($101.58\ m^2/g$) > 70-ZnMgO ($58.99\ m^2/g$) > 30-ZnMgO ($29.93\ m^2/g$) > pure ZnO ($19.31\ m^2/g$). The surface area increased gradually with the content of Mg element increasing, however decreased while the content of Mg element exceeding 50% in the precursor. The reason that the surface area 70-ZnMgO decreased may be contributed to the MgC_2O_4 covered on the ZnMgO, which resulted to decrease the pore area. From the pore size distribution curves which inset in Fig. 5, all the pores on these materials are less than 10 nm. In addition, the hysteresis loops (typical type H4 loop) on these N_2 adsorption/desorption isotherms can be found, meaning that the pores on these materials are formed by particles accumulation. 50-ZnMgO shows a $101.58\ m^2/g$ BET value, which is much higher than pure ZnO (5.26 times higher) and other samples with different Mg alloy amount. As shown in Fig. 3D, 50-ZnMgO shows the highest photocatalytic water reduction performance, which performance is near 100 times higher than that of the pure ZnO photocatalyst. Thus, except the negative moved CB potential, bigger surface area also a positive factor to improve the photocatalytic water reduction performance due to the higher surface reaction sites. However, as shown in Fig. 3D, there is just a litter photocatalytic performance difference between 30-ZnMgO and 50-ZnMgO, and the BET value of 30-ZnMgO is $58.99\ m^2/g$ which is approximate half of 50-ZnMgO, so the surface area can influence the photocatalytic hydrogen evolution performance of ZnMgO solid, but not the main factor.In order to elucidate the doping effect of Mg further, the structures of the Zn-Mg-O (Fig. 6) were optimized based on density functional calculations by using the CASTEP code [20] with the core orbitals replaced by ultrasoft pseudopotentials, and a kinetic energy cutoff of 310 eV. Exchange and correlation effects were described by the Perdew–Burke–Ernzerhof (PBE) generalized gradient approximation (GGA) [21].

Fig. 7 presented the band structure of pure ZnO and Z-Mg-O. As shown in Fig. 7, ZnO is a direct band gap semiconductor at G point with a band gap of 1.34 eV or so. And the band gap was found to be enhanced by the doping of Mg with the band gaps of 2.20, 2.58, 2.77 eV for the doped 30-ZnMgO, 50-ZnMgO and 70-ZnMgO,

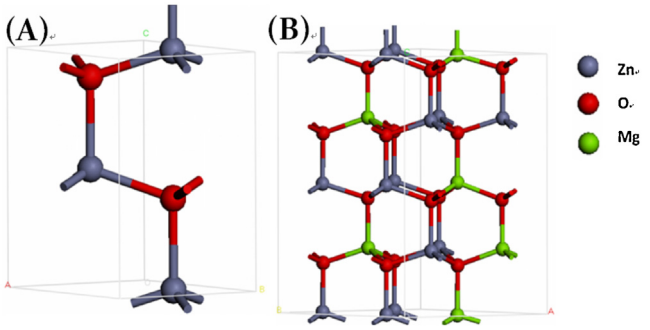

Fig. 6. (a) The conventional cell of ZnO. (b) The supercell of $Zn_xMg_{1-x}O$ (x = 0.3125).

respectively. And these results indicated a rule of that the higher the doping level is, the bigger the band gap is, which is consistent well with the literatures' findings [22] and the gradual increasing blue shift of absorption edges of the Mg doped ZnO relative to that of the pure one following the doping level enhancement in the UV-vis diffuse reflection spectrum (DRS) experiment (Fig. 3A).

Moreover, in order to elucidate the catalytic activity change trend of the materials through Mg doping, the position of the band edges including valence band Maximum (VBM) and conduction band Minimum (CBM) were determined further by the following equations, [23]

$$E_{CBM} = \chi - E^e - 0.5E_g$$

$$E_{VBM} = E_g + E_{CBM}$$

where E_{CBM} and E_{VBM} are the potentials of the CB and VB edges, respectively, with respect to the normal hydrogen electrode (NHE); χ is the electronegativity of the semiconductor and equals to the geometric mean of the electronegativities of the compositions; E^e is the energy of free electron on the hydrogen scale (4.5 eV), and E_g is the bandgap of the semiconductor. Here, the experimental bandgaps of ZnO (3.18 eV), 30-ZnMgO (3.26 eV), 50-ZnMgO (3.32 eV) and 70-ZnMgO (3.35 eV) are adopted according to the experimental measurements (Fig. 3C). And the absorption edges are shown in Table 1.

Table 1
the calculated CBM and VBM based on band gap from experiments.

ZnMgO	ZnO	30-ZnMgO	50-ZnMgO	70-ZnMgO
CBM (eV)	−0.31	−0.49	−0.61	−0.71
VBM (eV)	2.87	2.77	2.71	2.64

It is found that (Table 1) for the Mg doped ZnO materials the band gap increase brings a more negative CBM, and a more negative VBM for it, which indicated a better reduction and a still good enough oxidation capability. And the band edges shift amplitude was found to positively correlate with the doping level, following a rule of the higher the doping level, the larger the band edge movement. And these theoretical findings also shared a relatively good consistent with experimental evaluation on band edges displaying in Fig. 3C. Moreover, it is indicated in Table 1 that the change amplitude is about 2 times larger for the CBM than for the VBM. So the enhancement of activity which was due to doping is mainly embodying in the negative shift of the CBM and Mg doping would mainly bring a large enhancement on the reduction capability of ZnO, which is just the pursuit for H_2 production. Then results of calculation here confirmed the experimental findings of that the doping of Mg can enhance photocatalytic hydrogen evolution capacity of ZnO obtained above well.

4. Conclusion

In summary, we found a feasible method to prepare a hierarchic nanorod ZnMgO solid solution photocatalyst, and the energy band structure of ZnO can be adjusted by controlling the Mg doping con-

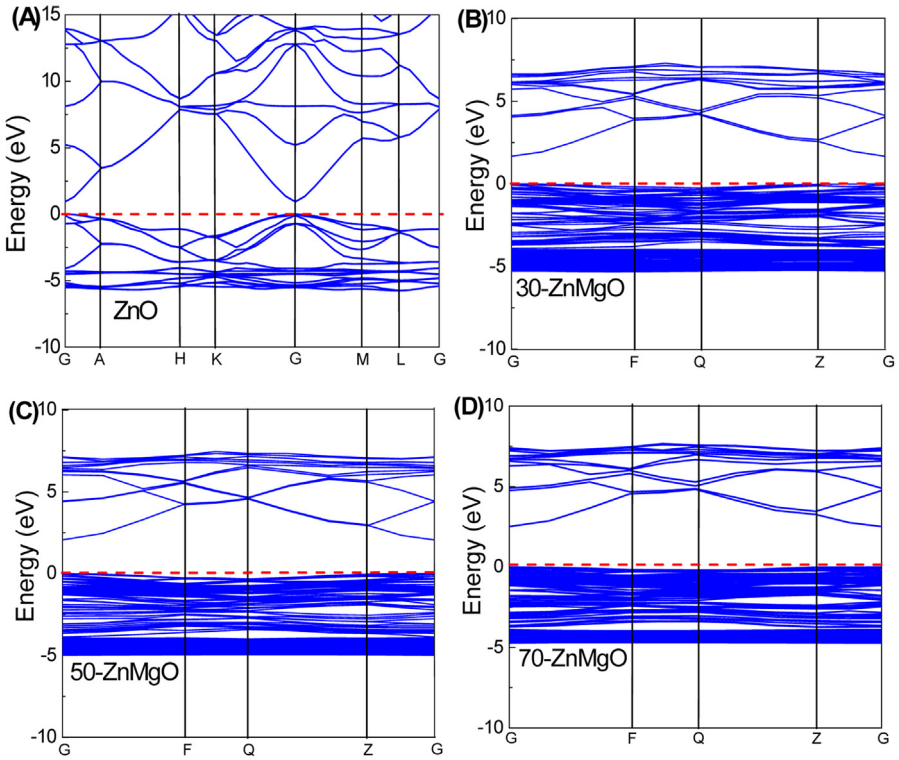

Fig. 7. The band structures for pure and Mg-doped ZnO. The dashed lines symbolize the Fermi levels which are set as 0 eV.

tent to improve the photocatalytic water splitting performance of this photocatalyst. In addition, based on the energy band structure of as-prepared ZnMgO solid solution in this study, we can develop more visible-light-responsive solid solution photocatalysts, such as ZnMgON, ZnMgOS etc, in the future.

Acknowledgements

The project was supported by National Natural Science Foundation of China (Grant no. 41506093) and The Open Fund of Key Laboratory of Marine Environmental Corrosion and Bio-fouling, Institute of Oceanology, Chinese Academy of Sciences

Appendix A. Supplementary data

Supplementary data associated with this article can be found, in the online version, at http://dx.doi.org/10.1016/j.apcatb.2017.04.079.

References

[1] M. Shao, F. Ning, M. Wei, D.G. Evans, X. Duan, Adv. Funct. Mater. 24 (2014) 580–586.
[2] B. Zhang, Z. Wang, B. Huang, X. Zhang, X. Qin, H. Li, Y. Dai, Y. Li, Chem. Mater. 28 (2016) 6613–6620.
[3] K.M. Lee, C.W. Lai, K.S. Ngai, J.C. Juan, Water Res. 88 (2017) 428–448.
[4] Y. Chen, H. Zhao, B. Liu, H. Yang, Appl. Catal. B 163 (2015) 189–197.
[5] J.M. Wu, W.T. Kao, J. Phys. Chem. C 119 (2015) 1433–1441.
[6] A. Sirelkhatim, S. Mahmud, A. Seeni, N.H.M. Kaus, L.C. Ann, S.K.M. Bakhori, H. Hasan, D. Mohamad, Nano-Micro Lett. 7 (2015) 219–242.
[7] H. Pan, N. Misra, S.H. Ko, C.P. Grigoropoulos, N. Miller, E.E. Haller, O. Dubon, Appl. Phys. A-Mater. 94 (2009) 111–115.
[8] Y.J. Yuan, F. Wang, B. Hu, H.W. Lu, Z.T. Yu, Z.G. Zou, Dalton Trans. 44 (2015) 10997–11003.
[9] D. Bao, P. Gao, X. Zhu, S. Sun, Y. Wang, X. Li, Y. Chen, H. Zhou, Y. Wang, P. Yang, Chem. – A Euro. J. 21 (2015) 12728–12734.
[10] K. Maeda, K. Teramura, D. Lu, T. Takata, N. Saito, Y. Inoue, K. Domen, Nature 440 (2006) 295.
[11] X. Hou, S. Jiang, Y. Li, J. Xiao, Y. Li, Inter. J. Hydro. Energy 40 (2015) 15448–15453.
[12] N. Minegishi, J. Kubota, K. Domen, Chem. Sci. 4 (2013) 1120–1124.
[13] F. Zhang, A. Yamakata, K. Maeda, Y. Moriya, T. Takata, J. Kubota, K. Teshima, S. Oishi, K. Domen, J. Am. Chem. Soc. 134 (2012) 8348–8351.
[14] H. Fujito, H. Kunioku, D. Kato, H. Suzuki, M. Higashi, H. Kageyama, R. Abe, J. Am. Chem. Soc. 138 (2016) 2082–2085.
[15] K. Ueda, T. Minegishi, J. Clune, M. Nakabayashi, T. Hisatomi, H. Nishiyama, M. Katayama, N. Shibata, J. Kubota, T. Yamada, K. Domen, J. Am. Chem. Soc. 137 (2015) 2227–2230.
[16] J.C. Hill, Y. Ping, G.A. Galli, K.S. Choi, Energy Environ. Sci. 6 (2013) 2440–2446.
[17] V. Etacheri, R. Roshan, V. Kumar, A.C.S Appl Mater Interfaces 4 (2012) 2717–2725.
[18] E. Diler, S. Rioual, B. Lescop, D. Thierry, B. Rouvellou, Thin Solid Films 520 (2012) 2819–2823.
[19] H. Nouri, A. Habibi-Yangjeh, M. Azadi, J. Photochem. Photobiol A 281 (2014) 59–67.
[20] M.D. Segall, P.L.D. Lindan, M.J. Probert, C.J. Pickard, P.J. Hasnip, S.J. Clark, M.C. Payne, J. Phys.: Condens. Matter 14 (2002) 2717.
[21] J.P. Perdew, K. Burke, M. Ernzerhof, Phys. Rev. Lett. 77 (1996) 3865–3868.
[22] X.D. Zhang, M.L. Guo, C.L. Liu, L.A. Zhang, W.Y. Zhang, Y.Q. Ding, Q. Wu, X. Feng, Eur. Phys. J. B 62 (2008) 417–421.
[23] K.N. Ding, B. Chen, Z.X. Fang, Y.F. Zhang, Theor. Chem. Acc. 132 (2013) 1352.